Development and Validation of Effective Computational Strategies for the Study of Metal Nitroxide Complexes

Andrea di Matteo and Vincenzo Barone*

Dipartimento di Chimica, Università di Napoli "Federico II", via Mezzocannone 4, I-80134 Napoli, Italy

Received: April 6, 1999; In Final Form: July 9, 1999

The structures and spectromagnetic properties of some model copper nitroxide complexes were studied by both density functional and multireference post-Hartree−Fock models in order to assess the reliability of different computational procedures. Next, the most promising density functional was employed for a systematic study of the effect of structural parameters and choice of the model system on the magnetic properties of copper nitroxides. These results provided the reference data for the extension of our recent nitroxide force field (*J. Am. Chem. Soc.* **1998**, *120*, 7069) to copper complexes. The resulting computational tool (consisting of magnetic properties evaluated by density functional methods possibly using geometries optimized by cheaper moleculear mechanics approaches) seems particularly effective and well suited for systematic use also by nonspecialists. Extension to other metals is quite straightforward along the same lines.

1. Introduction

The experimental investigation of exchange interactions between magnetic centers both in a vacuum and in condensed phases represents one of the main research topics in modern chemistry.[1]

For instance, magnetostructural correlations are widely used to interpret the magnetism of solids[2] and to develop synthetic strategies affording compounds with suitable magnetic properties. Furthermore, in bioinorganic chemistry the understanding of the magnetic interactions between metal centers provides information about the coordination environment and gives assessments about the geometry of active sites in enzymes.[3]

In the past few years, a number of magnetic systems containing organic free radicals (like nitroxide derivatives) and paramagnetic transition metal ions have been synthesized as possible precursors for ferromagnetic materials.[4] Here, we will concentrate on copper(II) complexes. Although both σ and π bonding may occur between the nitroxide and the metal, only one example of the latter situations has been characterized, namely, the $CuBr_2(TEMPO)$[5] complex (TEMPO is 2,2,6,6-tetramethyl-piperidinyl-1-oxy) in which the ligand is bound in a η^2 fashion. In all the other reported nitroxide complexes the free radical is bound to the metal through the oxygen atom only.[6] The complexes can be grouped into two classes, each possessing characteristic structural and magnetic features. Complexes with short-bonded equatorial ligands exhibit strong antiferromagnetic coupling,[7] while those containing a long-bonded axial nitroxide[8] have ferromagnetic behavior. Schematic drawings of both classes of complexes are shown in Figure 1.

Although X-ray structures are available for complexes of each class, their magnetic characteristics are often difficult to analyze from an experimental point of view. For instance in the case of equatorial complexes Gatteschi et al.[6] emphasize the difficulty in obtaining reliable *J* values, since the magnetic susceptibility is essentially constant in the entire temperature range. At the same time the computation of reliable magnetic couplings

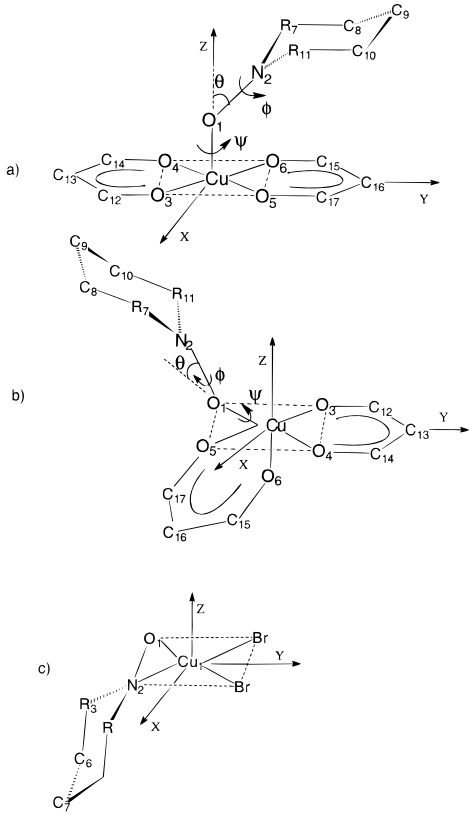

Figure 1. Schematic drawing of complexes studied in the present work together with labeling of atoms and main geometrical parameters. In the simplified models R groups are H atoms or methyl groups in place of methylene groups.

represents a severe challenge for quantum mechanical methods since they are obtained as differences between much larger quantities where both dynamic and non dynamic correlation effects play a significant role.

Since the chemically interesting systems are quite large and the magnetic properties are quite demanding from a computational point of view, two limiting strategies have been employed.

* Corresponding author. Voice: +39-081-5476503. Fax: +39-0815527771. E-mail: enzo@chemna.dichi.unina.it.

10.1021/jp991151v CCC: $18.00
Published on Web 09/08/1999

Either low-level quantum mechanical approaches have been employed to study real systems at experimental geometries[9,10] or very small models of high symmetry have been selected,[11] which allow the use of the refined post-Hartree−Fock methods needed to obtain accurate magnetic properties.[12,13] Although these approaches have provided a number of interesting results, the structures of magnetic systems are often only poorly characterized from an experimental point of view and environmental effects (solvent, crystal) cannot be neglected in some circumstances.[14] At the same time, too simple molecular models could miss some structural feature needed to tune the magnetic interactions.[11]

These considerations point out the need for a comprehensive theoretical approach allowing the geometry optimization of large structures for condensed phases also. Thanks to the recent advances in algorithms and hardware, geometrical structures can be fully optimized by quantum mechanics (QM) or molecular mechanics (MM) models including, when needed, a proper treatment of environmental effects.[15] Unfortunately, refined QM computations are still too expensive for molecules containing several heavy atoms. On the other hand, the MM approach rests on the availability of simple and accurate force fields for the description of potential energy surfaces governing conformational transitions.[16,17] Last generation density functional (DF) methods could provide an effective solution for these problems, since they generally couple reliable results with reasonable computer times. At the same time, more refined computations can be performed using DF geometries, and force fields for new systems can be optimized with reference to DF computations for a suitable training set. Next, powerful composite methods (ONIOM, QM/MM, etc.) can be employed for investigating very large compounds, possibly including bulk solvent effects by continuum models.[15] Some attempt in this direction has been done for biradicals[12,13,18] and metal dimers,[19,20] but comparable studies are still lacking in the field of metal radical complexes.[20]

The present study is devoted to the development and validation of integrated computational tools for the study of magnetic properties in large size metal nitroxide systems. The paper is organized as follows. After a short description of the computational details and theoretical background, two sections are devoted to the validation of the DF approach for the study of structural and magnetic properties both of model systems and of more realistic complexes. In particular, in the first section we present a comparison between methods based on the density functional theory and multiconfigurational methods of reduced dimension for model Cu(II) complexes interacting with the simplest nitroxide radical (H_2NO). In the second section we study the geometrical structure and magnetic correlations of [$(acac)_2Cu$−TEMPO] and Br_2Cu−TEMPO, where acac represents the acetylacetonate ligand.[20] In the last section we report the essential details of the extension of our nitroxide force field to copper complexes and discuss a few applications of the new QM/MM approach.

2. Theoretical Background

Quantitative calculations of the magnetic exchange interactions require an accurate description of the multiplet structure for the ground and the lowest excited states of the system at hand. This corresponds to the evaluation of the energies of all the spin states resulting from different occupations of a set of one-electron levels. Although the highest spin (HS) state has a single-determinant representation, this is not true for the other spin states. For instance, in the simple case of two active electrons, such as in copper nitroxide complexes, three different configurations give rise to low-lying singlet states, while only one configuration is involved in the triplet state.

The contribution of these excited configurations to the lowest singlet state is important, and neglecting them leads to an underestimation of the singlet−triplet gap. This problem is minimized by the presence of strong antiferromagnetic couplings leading to large energy gaps between the ground and the excited singlet configurations. In such circumstances a single-determinant wave function is close to the right solution for the ground state, whereas the situation is much more involved in the more interesting situation of small magnetic couplings. A number of studies have shown that these latter cases can be treated more effectively by computing the energy of a fictive electronic state intermediate between high- and low-spin eigenstates. In particular, when considering two active electrons, the unrestricted solution for the singlet state (referred to in the following as the broken symmetry,[21] BS, solution) is the sum of two components: a triplet (Ψ_T) and a singlet (Ψ_S),

$$\Psi_{BS} = a\Psi_S + b\Psi_T \tag{1}$$

with energy

$$E_{BS} = a^2E_S + b^2E_T \tag{2}$$

and of course,

$$a^2 + b^2 = 1 \tag{3}$$

Therefore, the singlet−triplet gap (usually denoted as $2J$) can be written as

$$2J = E_S - E_T = \frac{E_{BS} - E_T}{1 - b^2} \tag{4}$$

Since the expectation value of the spin square operator $\langle S^2\rangle$ is 0 for the true singlet and 2 for the triplet, b^2 is nothing else but half the expectation value of S^2 for the broken-symmetry state:

$$b^2 = \frac{1}{2}\langle\Psi_{BS}|S^2|\Psi_{BS}\rangle \tag{5}$$

As a consequence, when the BS solution is the average of singlet and triplet states (i.e., the two magnetic orbitals are degenerate and orthogonal), we get

$$2J = 2(E_{BS} - E_T) \tag{6}$$

which is the original result by Noodleman.[21] Equation 4 for the more general case of nonorthogonal orbitals has been employed several times with remarkable results.[22−26] In particular, it has been given in a very similar form by Ovchinnikov and Labanowski,[25] whereas Yamaguchi and co-workers use (rewriting eq 4b of ref 24 with our notation)

$$E_S = \frac{E_{BS} + \langle S^2\rangle_{BS}}{\langle S^2\rangle_T - \langle S^2\rangle_{BS}}(E_{BS} - E_T) \tag{7}$$

Using eqs 3, 5, and $\langle S^2\rangle_T = 2$, we get

$$E_S = \frac{2E_{BS}(a^2 + b^2) - 2b^2E_T}{2(1 - b^2)} = \frac{E_{BS} - b^2E_T}{1 - b^2} \tag{8}$$

which leads directly to eq 4.

To proceed further, we recall that for a singlet state[27]

$$\langle S^2\rangle_{BS} = \frac{N}{2} - \sum_{i\alpha}^{N/2}\sum_{j\beta}^{N/2} |S_{ij}^{\alpha\beta}|^2 \quad (9)$$

where N is the number of electrons and $S_{ij}^{\alpha\beta}$ is the overlap between the spin orbitals $|i\alpha\rangle$ and $|j\beta\rangle$ referring to opposite spins. Neglecting next spin polarization (i.e., assuming that the overlap between spin orbitals for opposite spins is negligible except for the magnetic spin orbitals $|a\rangle$ and $|b\rangle$), we get

$$\langle S^2\rangle_{BS} = 1 - S_{ab}{}^2 \quad (10)$$

and

$$2J = 2\frac{E_{BS} - E_T}{1 + S_{ab}{}^2} \quad (11)$$

as given by Noodleman and Norman[21] and in ref 26. In the following we will use the more accurate eq 4, which can be also generalized for arbitrary mixtures of spin states.[25] Although computation of $\langle S^2\rangle$ in DF methods is not free from difficulties,[28] it has been repeatedly shown that the use of eq 9 (i.e., of the Slater determinant built with the Kohn−Sham spin orbitals) provides sensible results. In any case, the same reservation (i.e., that a wave function is not explicitly needed in DF approaches) would impede also use of eq 11.

3. Computational Details

All the quantum mechanical computations have been performed with the help of a locally modified version of the GAUSSIAN 98 package[23] using for Cu and Br quasi relativistic effective core potentials (ECP),[30] in which 19 and 7 electrons are left out of the core for Cu and Br, respectively. Valence electrons have been described by the so-called Lanl2dz[30] basis set augmented by polarization functions on the Br atom (ζ_d = 0.451). The all-electron 6-31G* basis set[31] has been used for H, C, N, and O.

We have employed both conventional DF methods and HF/DF hybrids. In the former case, we have considered Xα and SVWN local models[32] together with generalized gradient approximations (GGA) due to Becke (B)[33] or to Perdew and Wang (PW)[34] for the exchange and to Lee, Yang, and Parr (LYP)[35] or to Perdew and Wang (PW)[36] for the correlation. However, we have replaced the original PW exchange functional by our mPW model, which has an improved long-range behavior.[37]

Following current practice, conventional functionals are denoted by linking the acronyms of their exchange and correlation parts (e.g., BLYP or PWPW), whereas for hybrid models a digit (indicating the number of additional parameters) separates the exchange and correlation acronyms. The popular B3LYP hybrid[31,38] corresponds to

$$E_{xc}^{B3LYP} = a_{x0}E_x^{LSD} + (1 - a_{x0})E_x^{HF} + a_{x1}\Delta E_x^{B} + (1 - a_c)E_c^{LSD} + a_cE_c^{LYP} \quad (12)$$

where the local contribution to the exchange energy (E_x^{LSD}) is that of the uniform spin-polarized electron gas,[31,32] the local correlation component (E_c^{LSD}) is represented by the Vosko−Wilk−Nusair (VWN) parametrization,[32] and the three semiempirical constants are those determined in the original work of Becke,[38] i.e., a_{x0} = 0.80, a_{x1} = 0.72, and a_c = 0.81. Using, instead, a single parameter to mix HF and DF exchanges,[39] we obtain the B1LYP and mPW1PW models[33]

$$E_{xc}^{B1LYP} = 0.25E_x^{HF} + 0.75E_x^{B} + E_c^{LYP} \quad (13)$$

$$E_{xc}^{mPW1PW} = 0.25E_x^{HF} + 0.75E_x^{mPW} + E_c^{PW} \quad (14)$$

All the geometrical parameters of the complexes have been fully optimized at the B1LYP[37] level using an unrestricted formulation (UB1LYP) for triplet states and the analytical gradient procedure available in the GAUSSIAN 98 package. All the magnetic properties have been computed using these geometries. We are well aware that unrestricted geometry optimizations can lead to serious artifacts for strongly spin contaminated cases, but all the triplet states considered in the present work are virtually uncontaminated ($2.0 < \langle S^2\rangle < 2.01$ estimating $\langle S^2\rangle$ from Kohn−Sham orbitals).

By use of the same geometries, multireference computations have been performed using the CAS facility of the G98 package and a modified version of the CIPSI package,[40] whereas molecular mechanics geometry optimizations have been performed using our modified MM+[41,42] force field included in the Hyperchem package.[43]

4. Results and Discussion

As mentioned above, we have studied two different geometrical situations corresponding to axial and equatorial positions of the nitroxide ligand, respectively (see Figure 1). In general terms the magnetic orbitals of $[(acac)_2Cu{-}ONH_2]$ complexes are essentially obtained from the singly occupied π^* orbital of the nitroxide radical and from one doubly occupied (FMO2) and one singly occupied (FMO1) orbitals of the Cu(acac)$_2$ fragment (see Figure 2).

In the axial complex FMO1 is generated by the antibonding interaction between the d_{xy} orbital of the copper atom and the sp^2 orbitals of oxygen atoms belonging to acac groups, whereas for symmetry reasons, the more stable fragment orbital (FMO2) is nothing but the d_{z^2} orbital of the Cu atom. On the other hand, in the equatorial complex both the d_{z^2} and d_{xy} orbitals of Cu can interact with the sp^2 orbitals of the oxygen atoms of acac groups, leading to more delocalized fragment orbitals. As a consequence, FMO1 is slightly less stable in the axial complex where antibonding interactions with four oxygen atoms are operative, whereas only three interactions of this kind are possible in the equatorial complex. At the same time, FMO2 is more stable in the axial complex, where it corresponds to the d_{z^2} Cu orbital, whereas an antibonding interaction with the axial oxygen of acac is possible in the equatorial complex. Thus, the splitting between fragment orbitals is significantly larger in the axial complex.

When interactions between Cu(acac)$_2$ and the nitroxide radical are switched on in the axial complex, a weak interaction is allowed between FMO2 and the NO π^* orbital, whereas FMO1 remains unaltered (see Figure 2). Of course, the two magnetic orbitals (HOMO and LUMO) have different symmetries but quite close orbital energies. In this case the two singlet states having both electrons in the same orbital correspond to excited charge-transfer configurations, and the ground singlet state has one electron in each magnetic orbital.

In the equatorial complex both fragment orbitals have a nonzero overlap with the NO π^* orbital; then bonding and antibonding interactions between the partners lead to a significant splitting of the resulting frontier orbitals (HOMO and LUMO) and, as a consequence, to antiferromagnetic behavior.

These qualitative considerations will be used in the following to analyze the quantitative results obtained by different methods.

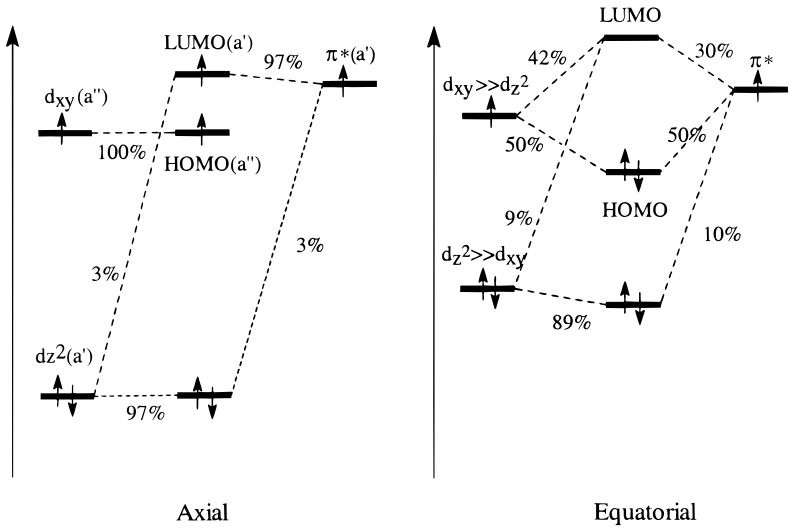

Figure 2. Schematic interaction scheme for the formation of axial and equatorial complexes.

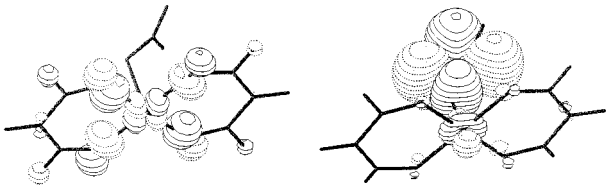

Figure 3. Magnetic orbitals of the axial $Cu(acac)_2H_2NO$ complex.

TABLE 1: Singlet−Triplet Separation (cm^{-1}) Computed for the Axial Conformer of [$(acac)_2$-Cu−ONH_2]

method of calculation	$2J = E_S - E_T$ (cm^{-1})
Xα	190
SVWN	151
BLYP	134
B3LYP	80
B3PW91	110
B1LYP	91
mPW1PW	88
CAS(2,2)/ROHF	71
exptl[a]	10−70

[a] From ref 6.

(a) Validation of Electronic Models. *Axial Complex*. In the axial complex the coordination around the copper(II) ion is a distorted square pyramid with the O atoms of the acetylacetonate fragments occupying the equatorial positions and the O atom of the nitroxide ligand binding in the axial position.[7a]

Three positions of ONH_2 with respect to the CuO_4 plane have been considered as represented by different values of the ψ angle (see Figure 1). Experimentally, it was found that the triplet state is always the ground state irrespective of the ψ angle value.[6]

As mentioned above, the HOMO is an antibonding Cu−O orbital mainly localized onto the $3d_{xy}$ metal orbital, which points toward the equatorial oxygen atoms, while the LUMO is essentially formed by a N−O π^* orbital almost equally delocalized onto the N and O atoms but with a nonnegligible contribution of the d_{z^2} orbital of copper (Figure 3).

The results of the calculations for $\psi = 90°$ are reported in Table 1. CAS(2,2)/ROHF and BS-DFT calculations have been performed also for $\psi = 0°$ and 45°. In all cases a ferromagnetic ground state is computed and the S−T splitting is almost independent of the ψ angle, in agreement with experimental findings.[6] Since the system has a fairly strong ferromagnetic behavior, electronic exchange plays the dominant role in determining the S−T splitting. Therefore, both DF models and simple ab initio approaches can be used to describe the magnetic structure of these systems.

From a quantitative point of view, the couplings obtained by local functionals (190 and 151 cm^{-1} at the Xα and SVWN level, respectively) are reduced including gradient corrections (134 cm^{-1} at the BLYP level) and finally led to close agreement with experimental results when adding also some exact exchange (80 and 91 cm^{-1} at the B3LYP and B1LYP levels, respectively). At the same time, the detailed form of the correlation functional does not play a negligible role (80 and 110 cm^{-1} at the B3LYP and B3PW level, respectively). As is well-known, the PW correlation functional includes, contrary to the LYP one, the contribution of electrons with parallel spins, thus increasing the stabilization of the triplet state. As a consequence, the S−T energy gap for ferromagnetic systems provided by the B3PW functional is larger than its B3LYP counterpart.

The B3LYP and B1LYP energy gaps are very close to experimental values, but the triplet state is slightly more stable at the B1LYP level because of the larger contribution of HF exchange (25% vs 20%).

Equatorial Complex. In this complex the nitroxide group is equatorially bonded with a short Cu−O distance (see Figure 1). The principal distortion from an ideal geometry is the displacement of one of the O atoms out of the plane containing the basal square of the pyramid.[44] At the same time the axial oxygen atom is displaced from its ideal site leading to an O−Cu−O angle (110.8°) significantly larger than the standard value of 90°. In our calculations we have employed an idealized square-pyramid structure without these distortions induced by the crystal environment.

It has not been possible to determine experimentally a reliable magnetic coupling in this and related systems, since both experimental and theoretical considerations suggest that the magnetic coupling is strongly antiferromagnetic ($|2J| > 500$ cm^{-1}). This is related, of course, to the significant overlap between the d_{xy} orbital of the Cu atom and the π^* orbital of the nitroxide radical, leading to the HOMO and LUMO shown in Figure 4.

Results of CAS(2,2)/ROHF and DFT computations with different functionals are displayed in Table 2. This is a case in which the standard BS formalism overestimates the magnetic

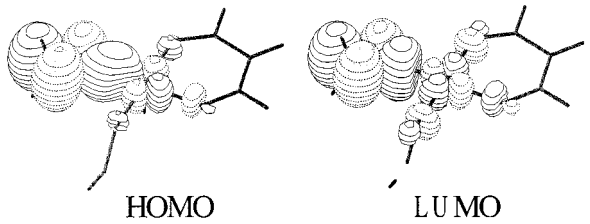

Figure 4. Magnetic orbitals of the equatorial $Cu(acac)_2H_2NO$ complex.

TABLE 2: Singlet−Triplet Separation (cm^{-1}) Computed for the Equatorial Conformer of [$(acac)_2$-Cu−ONH_2]

method of calculation	$\langle S^2 \rangle$	$2J = E_S - E_T$ (cm^{-1})[a]
Xα	0.0	−1737
SVWN	0.0	−2846
BLYP	0.0	−1772
B3LYP	0.8344	−1402 (−2407)
B3PW91	0.8342	−1372 (−2366)
B1LYP	0.8735	−1342 (−2382)
mPW1PW	0.8764	−1309 (−2331)
CAS(2,2)/ROHF		−1900

[a] In parentheses values corrected for overlap.

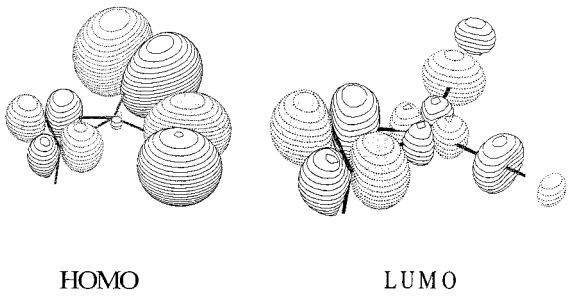

Figure 5. Magnetic orbitals of the $CuBr_2H_2NO$ complex obtained at the B1LYP level.

coupling by more than 50% because the overlap integrals between the magnetic orbitals are quite large.

The complex is strongly antiferromagnetic, and as expected, the magnetic coupling increases in absolute value when overlap effects are included in the BS formalism. Given the dimension of the system, we could not perform an accurate calculation of magnetic exchange; nevertheless, DFT and CAS(2,2) results are comparable.

The values obtained by functionals including some exact exchange (B3LYP and B3PW) are close to each other, while the BLYP magnetic coupling is significantly smaller; at the same time the detailed form of the correlation functional plays only a minor role, as shown by the very similar B3LYP and B3PW results. Like in the axial model, the B1LYP functional increases the stability of the triplet state with respect to B3LYP because of its larger content of HF exchange.

η^2-Complex. The particular diamagnetism of this system is a direct consequence of the multicentered linkage delocalized over the five atoms of the coordination plane.[45] The LUMO orbital (see Figure 5) has antibonding Br−Br and Cu−Br character with a large weight of p orbitals of Br atoms and, at the same time, an antibonding interaction between the NO π^* and the metal d_{xy} orbitals. The HOMO (see Figure 5) is a nonbonding orbital with large weights on both Br atoms and the NO π^* orbital.

The magnetic exchange couplings, calculated at the ab initio and DFT levels, are collected in Table 3. The result obtained by a local functional (SVWN, −7332 cm^{-1}) is reduced in absolute value including gradient corrections (BLYP, −6600 cm^{-1}), and even more by adding some exact exchange (B3LYP, −4068 cm^{-1}; B3PW91, −4075 cm^{-1}; B1LYP, −3600 cm^{-1}; mPW1PW, −3647 cm^{-1}).

TABLE 3: Singlet−Triplet Separation (cm^{-1}) Computed for the $CuBr_2$−ONH_2 Molecule

method of calculation	$\langle S^2 \rangle$	$CuBr_2$−ONH_2 $2J = E_S - E_T$ (cm^{-1})[a]
Xα	0.0	−6100
SVWN	0.0	−7332
BLYP	0.0	−6600
B3LYP	0.2346	−4068 (−4785)
B3PW91	0.2346	−4079 (−4796)
B1LYP	0.3596	−3600 (−4389)
mPW1PW	0.3660	−3647 (−4463)
CISD		−5530
CISD(all electron)		−5659
CCSD		−5371
CAS(2,2)/ROHF		−9825
CAS(10/6)		−10502
CIPSI		−11800

[a] In parentheses values corrected for overlap.

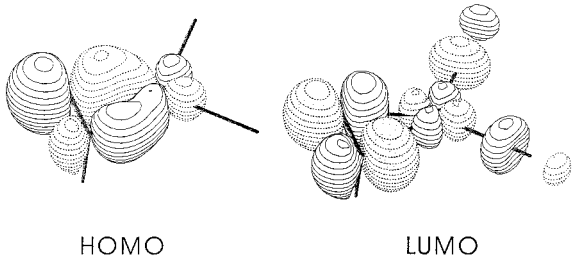

Figure 6. Magnetic orbitals of the $CuBr_2H_2NO$ complex obtained at the CAS(2,2) level.

As shown in Table 3, increasing the weight of exact exchange in the functionals, one observes a stabilization of the triplet state with respect to the values obtained at the BLYP and SVWN levels. CISD calculations for the singlet state have been performed correlating all the occupied valence orbitals with the LUMO orbital. The lowest triplet state remains unaffected by a similar expansion because of the Brillouin theorem.

The singlet−triplet energy separation calculated at this level is in good agreement with the results obtained by B3LYP and B1LYP models including a proper treatment of overlap. We have also performed calculations on the singlet state by both CAS(2,2) and CAS(10,6) approaches. In the first case we have introduced the nondynamic correlation only between the HOMO and LUMO orbitals, while in the second case we have included, together with the LUMO orbital, also the five highest occupied valence orbitals having the same symmetry. The values of both CAS computations are very similar and indicate a strong antiferomagnetic behavior. The magnetic orbitals obtained by multiconfigurational methods are shown in Figure 6.

Unlike the single-determinant approaches (HF, DFT), in the MCSCF formalism the frontier orbitals are typical orbitals with bonding and antibonding interactions between Cu and NO fragments. In particular, the LUMO is very similar to that calculated with the HF and DFT methods, while the HOMO becomes a bonding orbital with large weights both of the Cu atom and of the NO π^* orbital.

This trend can explain both the particular antiferromagnetism of η^2 systems and the large increase of the singlet−triplet gap when going from single reference methods (DFT, HF, CISD) to a multiconfigurational formalism. To better elucidate this point, we have performed also CIPSI[40,46] calculations using the CAS(2,2) natural orbitals of the singlet state. The singlet and triplet states belong to the same symmetry (A′), and thus, they

can be obtained by a single calculation. The final CIPSI magnetic coupling (obtained after several steps, where a threshold selects the determinants that contribute to the first-order wave function of the state studied until arrival at the convergence of the energy) is quite close to the CAS value ($2J = -11\,800$, $-10\,500$, and -9800 cm^{-1} by CIPSI, CAS(10,6), and CAS(2,2) methods, respectively).

In summary only multireference approaches give reliable results for this complex, since the orbitals provided by single reference procedures are not sufficiently reliable for the singlet state. However, also in this case DF methods provide reliable geometries (see below) that can then be employed in more refined computations of model compounds, the more so, since the magnetic properties obtained using H_2NO or the true TEMPO radical are very close.

(b) Geometric Structures and Magnetic Properties. In the previous section, we have shown that reliable magnetic properties can be obtained by hybrid HF/DF approaches using experimental geometric structures. However, in most cases these data are not available, so it is important to investigate if the same quantum mechanical methods are also able to provide good geometries. To this end we have selected the B1LYP method, which gives results close to the B3LYP approach with a reduced number of parameters. Geometries have been fully optimized at this level for the triplet state of the axial complex and for the singlet state of the equatorial complex, whereas the geometries of both states have been optimized for the η^2-complex. Note that, on the basis of some test computations, we have always replaced the four methyl groups of TEMPO by hydrogen atoms.

Axial Complex. The geometrical parameters of [(acac)$_2$Cu−TEMPO] have been optimized with the only constraint of C_s symmetry. In Table 4 the calculated geometrical parameters are compared with the X-ray data available for the bis(hexafluoroacetylacetonato)(4-hydroxy-2,2,6,6-tetramethyl-piperidinyl-*N*-oxy)copper(II) (TEMPO−OH).[7a]

All the B1LYP geometrical parameters are close to experimental values.[7a] In particular, the copper(II) ion is displaced out of the plane defined by the acetylacetonate oxygen atoms in the direction of the oxygen atom (O_1) of the nitroxide radical. At the same time, the acetylacetonate rings are slightly bent away from the axial site occupied by the nitroxide oxygen atom. Also, this small distortion is reproduced by our computations, since the B1LYP dihedral angle between these two planes (10°) is very close to the experimental value of 15°.

The optimized value of the θ angle (see Figure 1) is significantly larger than its experimental counterpart (53.7° vs 10°), but it is very similar to the value expected for an ideal coordination through a lone pair on an sp^2 hybridized nitroxide oxygen atom (60°).

In the crystal structure the O(nitroxide) and O(hydroxyl) atoms of the bridging ligand (TEMPO−OH) are axially coordinated to different metal ions, and this leads to a Cu−O−N angle much larger than that expected for an sp^2-hybridized oxygen atom. At the same time the particular conformation of the nitroxide radical in the crystal structure could induce both the unusual flatness of the six-member ring and the planarity of the nitrogen atom. In our case the geometrical structure of the TEMPO ligand is very similar to that found for the isolated molecule[47] except for an increase of the out-of-plane angle (τ) of the NO moiety (25° vs 16°).

The geometrical parameters of the acac fragment are very close to the values expected for this bidentate ligand, and they do not deserve special comment.

In a previous section we have already discussed the nature of the ferromagnetic interaction in the axial complex. The magnetic exchange computed for the geometry optimized at the B1LYP level indicates that the system is ferromagnetic and that this interaction is rather weak (50 and 43 cm^{-1} at the B1LYP and CAS level, respectively). The magnetic coupling is thus quite similar to that of the model studied in section A (50 vs 91 cm^{-1} at the B1LYP level), the difference being related to geometry optimization rather than to the use of different nitroxide radicals. In fact, when the geometry is frozen to that used in section A, the coupling obtained for the TEMPO radical (89 cm^{-1}) is nearly identical to that found for the H_2NO radical (91 cm^{-1}). Nevertheless, all these values are higher than the experimental result (13 cm^{-1}). We have tried to better elucidate this point by computing the magnetic coupling at different values of the θ angle. The most striking aspect of these computations is that the magnetic coupling decreases, increasing the θ angle, and for $\theta \approx 10°$ it becomes very close to the experimental value (15.0 vs 13.0 cm^{-1}). For $\theta = 0°$, the Cu−O_1−N_2 angle is 180°, so the π^* and d_{xy} orbitals are orthogonal to each other irrespective of the ψ and ϕ angles. As discussed in ref 4, in this case the antiferromagnetic contribution vanishes and a moderate ferromagnetic coupling develops. Thus, in this system the θ angle plays a key role in tuning the magnetic coupling, which shows, at the same time, an exponential dependence on the Cu−O_1 distance.

Equatorial Complex. In the experimental structure the molecule is a discrete five-coordinate monomer with a pair of chelating hfac ligands and a monodentate O-bonded nitroxide radical. On the basis of the bond angles at the copper atom, Lim and Drago[48] suggested that the coordination geometry is between square pyramidal and trigonal bipyramidal. Next Dickman et al.,[44] on the basis of the pattern of one long and four short Cu−O distances, suggested that the configuration is best described as distorted square pyramidal. We have used this latter configuration where the nitroxide group is equatorially bonded with a short Cu−O distance in a distorted square pyramid.

The nitroxide oxygen atom O_1 then occupies a basal coordination site and is nearly coplanar with Cu, O_4, and O_5, and these four atoms define the basal plane of the square pyramid. The principal distortion from local symmetry about Cu is a displacement of O_1 below the basal plane. This distortion is reflected in the O_3−Cu−O_5 and O_3−Cu−O_6 valence angles, whose computed values (158.6° and 106.3°, respectively) are not far from the experimental data (149.4° and 123.9°, respectively). All the other O−Cu−O angles are close to 90° or 180°. The TEMPO ligand is bound to Cu via a short Cu−O_1 bond whose length is quite close to the experimental value (1.950 vs 1.920 Å[44]). This arrangement provides the largest overlap between the nitroxide π^* orbital and the metal orbital pointing toward the oxygen atom. It is this overlap that leads to partial pairing of the unpaired electrons and contributes to the stability of the equatorial complex.

In contrast to the near-linear Cu−O−N angle of 170° discussed in the case of the axial complex, the angle in this molecule is 119.2°, not far from the experimental value of 123.9°.

The N−O_1 distance of 1.273 Å and the C−N−C angle of 119.3° are close to the values of 1.283 Å and 123.6° found in free TEMPO[42] and in the structure of the experimental complex. The ϕ dihedral angle (see Figure 1) of 81.4° is close to the experimental value of 85.1° and indicates that the O_1−C_7−C_{11} and Cu−O_1−N planes are nearly perpendicular.

As a last step, we tried to optimize the structure of the triplet

TABLE 4: Geometrical Parameters Optimized by B1LYP and MM Levels of the [Cu(acac)$_2$−TEMPO] for Both Conformations Are Compared with Experimental Values and with the Averaged Values Used in the Computations on the Model (See Text for Explanation)

		axial complex			equatorial complex		
geometrical parameter	models[a]	exptl[b]	B1LYP T	MM	exptl[c]	B1LYP S	MM
$Cu-O_4$	1.925	1.943	1.951	1.942	1.920	1.946	1.945
$Cu-O_3$		1.949	1.951	1.942	1.971	2.001	1.944
$Cu-O_5$		1.945	1.932	1.943	1.995	1.926	1.943
$Cu-O_6$		1.949	1.932	1.943	2.167	2.221	2.181
$Cu-O_1$	1.932 (2.303)	2.439	2.425	2.437	1.920	1.950	1.944
$C_{14}-O_4$		1.245	1.268	1.257	1.209	1.261	1.258
$C_{12}-O_3$	1.258	1.245	1.268	1.257	1.270	1.270	1.257
$C_{17}-O_5$		1.244	1.267	1.258	1.245	1.251	1.258
$C_{15}-O_6$		1.244	1.267	1.258	1.252	1.281	1.260
$C_{14}-C_{13}$	1.371	1.380	1.390	1.401	1.439	1.401	1.406
$C_{15}-C_{16}$		1.400	1.400	1.403	1.381	1.390	1.403
N_2-O_1	1.288	1.276	1.288	1.285	1.267	1.273	1.287
R_7-N_2		1.481	1.462	1.500	1.492	1.467	1.501
R_7-C_8		1.452	1.532	1.537	1.541	1.531	1.540
O_5-Cu-O_4	180.0 (90.0)	175.6	171.1	170.0	90.51	90.40	81.98
O_4-Cu-O_3	90.0	93.0	92.85	94.86	91.12	93.41	93.51
O_6-Cu-O_5	90.0	92.5	91.83	94.30	91.11	94.11	92.05
O_3-Cu-O_5	90.0 (180.0)	87.5	87.05	85.42	149.4	158.6	173.3
O_6-Cu-O_1	90.0	92.5	96.65	92.16	86.01	90.47	92.7
O_3-Cu-O_6	90 (180.0)				123.9	106.3	81.80
$Cu-O_4-C_{14}$	125.6	124.1	125.1	122.0	125.5	125.5	123.5
$Cu-O_3-C_{12}$					127.4	124.0	123.4
$Cu-O_5-C_{17}$		123.9	125.8	122.5	123.0	123.0	123.7
$Cu-O_6-C_{15}$					119.7	119.0	118.6
$O_4-C_{14}-C_{13}$	132.0	128.7	127.3	128.1	128.1	127.4	127.6
$O_3-C_{12}-C_{13}$					126.1	128.4	127.9
$O_6-C_{15}-C_{16}$		128.9	127.2	128.1	128.1	127.8	128.6
$O_5-C_{17}-C_{16}$					127.9	130.2	130.5
$C_{14}-C_{13}-C_{12}$	114.8	121.1	121.9	124.7	121.6	122.8	123.9
$C_{15}-C_{16}-C_{17}$					124.8	126.0	126.1
$Cu-O_1-N_2$[d]	121.1 (127.2)	170.1	126.3	125.8	123.8	119.2	123.5
$N_2-R_7-C_8$		113.0	110.9	109.7	108.6	110.2	109.6
$N_2-R_{11}-C_{10}$					109.0	110.7	109.8
$R_7-N_2-R_{11}$		126.7	118.3	122.7	124.3	119.3	123.4
$C_8-C_9-C_{10}$		123.4	110.7	108.9	109.6	110.5	107.6
$O_1-N_2-R_7$[e]	124.1	116.6	118.7	115.5	116.4	119.2	117.9
$C_9-C_{10}-R_{11}$		123.8	111.1	113.6	114.0	111.2	114.0
$R_7-C_8-C_9$					112.4	111.3	113.9
$C_{13}-Cu-C_{16}$		15.0	10.0	10.1			
$N-R_7-C_8-C_9$			−51.35	−48.43	−45.0	−51.7	−47.68
φ	90.0	85.88	77.88	98.01	85.1	81.42	88.30
ψ	90.0 (45.0)	72.3	45.0	45.0	84.7	90.0	90.0
τ[f]		5.0	24.9	28.5	16.0	17.1	12.0
$2J$ (cm^{-1})[g]			43.0	40.0		−3446	−3000
		13.0	15.0[h]	13.0[h]			

[a] Values for the equatorial form (when different from those for the axial form, they are given in parentheses). [b] From ref 7a. [c] From ref 39. [d] The angle is 180 − θ. [e] HNO angle of H_2NO. [f] Out-of-plane angle of the NO moiety. [g] Computed at B1LYP level. [h] Using the experimental value of θ.

state, but all our computations converged to the axial complex, suggesting that the equatorial structure is not a stationary point on the potential energy surface of the triplet state.

Calculation of magnetic exchange on the singlet geometry optimized at the B1LYP level confirms the results obtained for the model complex discussed in section a, namely, that the equatorial complex is strongly antiferromagnetic. However, the structure optimized at the B1LYP level has a S−T energy gap larger than the model complex (−3446 and −2383 cm^{-1} for the complex with the B1LYP geometry and for the model, respectively). On the other hand, substitution of the H_2NO radical in the model complex by TEMPO without reoptimizing the geometry has only a negligible effect on the magnetic coupling (−2383 and −2400 cm^{-1} for H_2NO and TEMPO, respectively). This suggests the presence of some significant magnetostructural relationship in this complex, which can be better investigated by computing the magnetic exchange for selected values of the three principal angles of coordination θ, φ, and ψ (see Figure 1).

In Figure 7 we plot the calculated $-2J$ values as a function of the θ angle for φ and ψ frozen at their optimized values. For $\theta = 0°$ the magnetic orbitals are very close to orthogonality and the system exhibits a weak ferromagnetic interaction. As soon as the θ angle is widened, the overlap increases and the magnetic behavior switches to an increasing antiferromagnetic regime. However, Figure 7 shows that a maximum is reached for $\theta = 60°$, which leads to the largest overlap between the two magnetic orbitals and agrees fairly well with the average of experimental values reported for equatorial complexes.[6] In contrast, an increase of φ results in a continuous increase of the overlap and, consequently, of the magnetic exchange (see Figure 8).

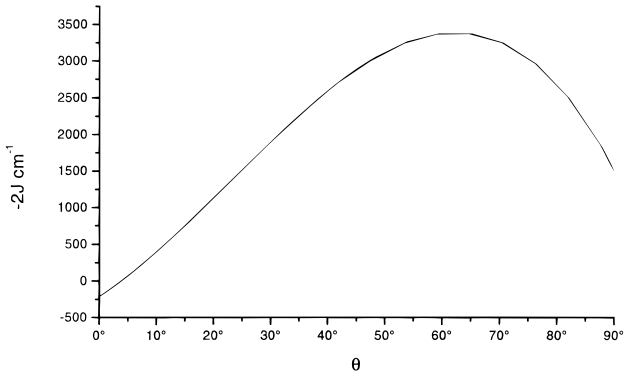

Figure 7. Variation of the magnetic coupling of the equatorial Cu(acac)$_2$H$_2$NO complex as a function of the θ angle (see Figure 1 for the definition of θ).

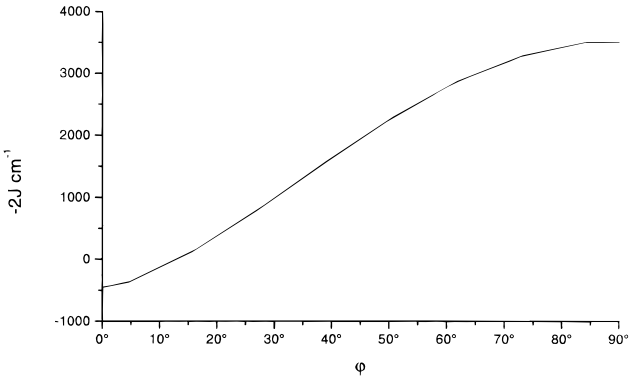

Figure 8. Variation of the magnetic coupling of the equatorial Cu(acac)$_2$H$_2$NO complex as a function of the ϕ angle (see Figure 1 for the definition of ϕ).

Finally, as already observed for the axial complex, variations of the ψ angle have little effect on the magnetic exchange and can be neglected.

η^2-Complex. The structural parameters obtained at the B1LYP level for $CuBr_2$(TEMPO) and two molecular models are summarized in Table 5 and show a good agreement with the available experimental data. Moreover, the lengths of the Cu−N and Cu−O bonds are very similar for all the nitroxide radicals, thus confirming that H_2NO is a suitable model for larger nonconjugated nitroxide radicals.

The structural parameters of the nitroxide fragment deserve some comment. The NO bond length is slightly longer and the usual pyramidal shape of the C_2NO moiety much more pronounced than in the free radical or in η^1-complexes.[5,47] This is not unexpected, taking into account that in $CuBr_2$(TEMPO) the nitrogen atom is also bound to the metal and that four-coordinated nitrogen atoms always have a nearly tetrahedral environment.

We have next optimized the geometry of the triplet state. The results of Table 5 show that the geometric parameters computed for the singlet and the triplet states are significantly different and that only the former ones are in agreement with experimental data. Thus, the structural predictions of the B1LYP model seem satisfactory and are already sufficient for discriminating between different electronic states on the basis of the agreement with experimental values.

The calculation of magnetic exchange interaction performed on the B1LYP geometrical structure indicates that, as discussed in previous sections, the complex is strongly antiferromagnetic and that the magnetic coupling obtained by multireference approaches is about twice the value computed at the B1LYP level. Also in this case the different shape of the magnetic orbitals obtained by the two computational models is responsible for this trend. Moreover, the magnetic couplings computed for the TEMPO complex are quite similar to those discussed in a previous section for the simplified model, thus confirming that the magnetic coupling is a local property almost independent of the nature of substituents of the NO moiety.

(c) QM/MM Approach. The geometric structures of axial and equatorial complexes have been fully optimized by MM+[41,42] calculations with the additional set of parameters introduced in ref 42 for nitroxide groups and here below for the Cu atom (see Table 6).

Starting from standard values, stretching and bending parameters involving the Cu atoms have been refined by trial and error until a good agreement with B1LYP results was reached. As discussed above, axial and equatorial coordinations of the nitroxide lead to two different spin states: a triplet state for the axial complex and a singlet state for the equatorial complex. Moreover, the optimization of the triplet state of the equatorial complex converged to the axial complex. We have used for the singlet state the standard values of the MM+ force field for the unstrained bond length and of the stretching force constant for M−O (where M is a metal ion). However, new parameters have been introduced for the M−O bond in the triplet state, for O−Cu−O bond angles where the oxygen atoms can belong either to acetylacetonate or to nitroxide moieties, and for the torsion angle between the oxygen of an acetylacetonate group and the sp^2 carbon of the other moiety. All the angle parameters are identical for different electronic states and have been obtained, together with bond parameters for the triplet, by fitting appropriate B1LYP computations. Electrostatic interactions have been described by atomic point charges using a unitary (i.e., vacuum) dielectric constant. For the TEMPO molecule we have used the same charges proposed in ref 42, while for the Cu(acac)$_2$ moiety they have been obtained by the restrained electrostatic potential (RESP) procedure recently introduced by Bayly et al.[49] The parameters ruling interactions between nonbonded atoms have been discussed in a previous work for the TEMPO molecule,[42] while for (acac)$_2$Cu we have used the standard values of the MM+ force field (which implies a vanishing van der Waals radius for the Cu atom).

The optimized geometrical parameters of axial and equatorial complexes are compared in Table 4 to experimental and B1LYP geometries. The results are quite satisfactory, and in particular, the Cu−O(nitroxide) bonds are well reproduced for both complexes. The bond angles of the Cu−O−N fragment and between the oxygen atoms of acetylacetonate or with nitroxide oxygen are close to experimental values. Moreover, the angles defining the coordination of the nitroxide radical to the metal (ψ and φ) are not far from experimental and density functional values. The principal distortions of the idealized symmetric structure discussed in previous sections are well reproduced by the MM calculation; for example, the value of the C_{13}−Cu−C_{16} angle issuing from MM computations is in good agreement with the B1LYP result (10.1° vs 10.0° by MM and B1LYP methods, respectively). The quite good agreement obtained for the other valence angles points out the reliability of the underlying force field.

Finally, magnetic couplings have been computed with the BS approach at the B1LYP level using MM+ structures. For both coordination modes, the values are close to those obtained using experimental and quantum mechanical geometries. In particular in the axial complex the 2J value is 40 cm^{-1}, close to the value computed at the B1LYP geometry (43 cm^{-1}) and

TABLE 5: Geometrical Parameters Optimized at the B1LYP Level for Two Models of $CuBr_2-ONR_2$ (R = H, CH_3) Are Compared to Available Experimental Data from Ref 5 (Bond Lengths Are in Angstroms and Angles in Degrees)

geometrical parameters	exptl[a]	$CuBr_2$(TEMPO) singlet state	R=R_3=H singlet state	R=R_3=H triplet state	R=R_3=CH_3 singlet state
$Cu-N_2$	1.998	2.060	1.957	2.088	1.968
$Cu-O_1$	1.860	1.905	1.917	1.959	1.920
N_2-O_1	1.304	1.307	1.329	1.354	1.320
$Cu-Br$[b]	2.270	2.330	2.301	2.422	2.314
N_2-Cu-O_1	39.30	38.22	40.1	38.9	39.7
$R-N_2-R$	123.1	123.0	115.3	113.2	117.1
$R-N_2-O_1$	114.8	114.9	116.2	113.9	115.8
Br−Cu−Br	106.5	109.1	104.6	79.4	104.5
$R-N_2-Cu-O_1$	107.8	107.9	109.6	104.4	109.2
τ[c]	29.0	28.2	38.6	48.7	35.9
N_2-R	1.540	1.531			
R_3-C_6	1.520	1.553			
R_3-C_4	1.538	1.538			
$R-C_5$	1.496	1.543			
$N-R_3-C_6$	106.7	108.1			
$R_3-C_6-C_7$	114.3	114.7			
$C_6-C_7-C_6$	108.9	109.8			
$C_4-R_3-C_5$	109.2	108.5			
$N_2-Cu-Br$	110.5	110.4			
$O_1-Cu-Br$	104.0	102.3			
$O_1-N_2-R_3-C_4$	48.24	51.35			
$O_1-N_2-R_3-C_5$	−70.8	−67.76			
$N_2-R_3-C_6-C_7$	−50.04	−47.78			
$2J$ (cm^{-1})[d]		−4507	−4389		−4270

[a] From ref 5. [b] Averaged on two Cu−Br bonds. [c] τ is the out of plane angle of the NO moiety. [d] Computed at the B1LYP level using eq 4.

TABLE 6: Optimized MM Parameters Involving Cu Species[a]

bond stretching[b]	R_0 (Å)	Kr (kcal mol^{-1})
Cu−O1[c]	1.94	500
Cu−OR(ax)	2.42	338
angle bendings	**θ_0 (deg)**	**Kθ (kcal mol^{-1} rad^{-2})**
Cu−OR−NR	120.0	64.8
O1−Cu−O1	90.0	72.0
OR−Cu−O1	90.0	72.0
torsion	**τ_0 (deg)**	**$V_2/2$ (kcal mol^{-1})**
O1−Cu−O1−CO	0.0	1.00

[a] See text for further details. [b] OR and NR are the atom types for nitroxide oxygen and nitrogen atoms, respectively. O1 and CO are the atom types for carbonyl oxygen and carbon atoms, respectively. [c] Standard MM+ value for M−O.

well within the experimental[6] range ($10 < 2J < 80$ cm^{-1}), while the equatorial complex shows a strong antiferromagnetic interaction (−3123 cm^{-1}) not far from the value computed using the B1LYP geometry (−3446 cm^{-1}).

5. Conclusion

This article is devoted to the development and validation of new effective computational strategies for the study of metal nitroxide complexes. Our results show that the broken-symmetry approach coupled to hybrid HF/DFT methods provides reliable magnetic properties in most situations. In extreme cases, a safer procedure is provided by multireference models of reduced dimensionality. Since both approaches can be well standardized and are currently feasible also for quite large systems, systematic studies can be performed also by nonspecialists provided that reliable structural data are available. In this connection, we have shown that the structures of triplet states obtained by unrestricted HF/DFT computations are in remarkable agreement with experimental values at least in the absence of strong spin contamination. These geometries can be used in the computation of magnetic properties whenever the singlet state is not much more stable than the triplet, i.e., in virtually all the situations that are interesting from a magnetic point of view. In other circumstances, geometry optimizations of the ground singlet state or of the broken-symmetry state can be more profitable and can be performed without special difficulties. Furthermore, solvent effects on both geometric and magnetic properties can be taken into account by our recent implementation of the polarizable continuum model.[13,15,42]

An even cheaper procedure consists of optimizing geometrical parameters at the MM level. Here, we have shown for the particular case of copper complexes that a quite straightforward extension of our nitroxide force field leads to reliable results. Work is in progress to extend this approach to other metals and to introduce the whole computational tool in a standard quantum mechanical package.

References and Notes

(1) Kahn, O. *Molecular Magnetism*; VCH: New York, 1993.

(2) (a) Milaeva, E. R.; Rubezhov, A. Z.; Prokof'ev, A. I.; Pkhlobystin, O.; Yu, O. *Usp. Khim.* **1982**, *51*, 1638. (b) Gatteschi, D. *Adv. Mater*. **1990**, *62*, 223. (c) Miller, J. S.; Epstein, A. *Angew. Chem., Int. Ed. Engl.* **1994**, *33*, 385.

(3) (a) Kitajima, N. *Adv. Inorg. Chem*. **1982**, *39*, 1. (b) Eaton, S. S.; Eaton, G. R. *Coord. Chem.Rev*. **1978**, *26*, 207. (c) Eaton, S. S.; Eaton, G. R. *Coord. Chem. Rev*. **1988**, *83*, 29.

(4) Caneschi, A.; Gatteschi, D. P.; Rey, P.; Sessoli, R. *Acc. Chem. Res.* **1989**, *22*, 392.

(5) Caneschi, A.; Grand, A.; Laugier, J.; Rey, P.; Subra, R. *J. Am. Chem. Soc.* **1988**, *110*, 2307.

(6) Caneschi, A.; Gatteschi, D.; Rey, P. *Prog. Inorg. Chem*. **1991**, *39*, 331.

(7) (a) Anderson, O. P.; Kuechler, T. C. *Inorg. Chem*. **1980**, *19*, 1417. (b) Grand, A.; Rey, P.; Subra, R. *Inorg. Chem*. **1983**, *22*, 391. (c) Caneschi, A.; Gattechi, D.; Laugier, J.; Rey, P. *J. Am. Chem. Soc.* **1987**, *109*, 2191. (d) Gattechi, D.; Laugier, J.; Rey, P.; Zanchini, C. *Inorg.Chem*. **1987**, *26*, 938.

(8) Caneschi, A.; Gatteschi, D.; Sessoli, R.; Hoffman, S. K.; Laugier, J.; Rey, P. *Inorg. Chem*. **1988**, *27*, 2390.

(9) Noodleman, L.; Peng, C. Y.; Case, D. A.; Mouesca, J. M. *Coord. Chem. Rev*. **1995**, *144*, 199.

(10) Gatteschi, D., Kahn, O., Miller, J. S., Placido, F., Eds. *Magnetic Molecular Materials*; NATO ASI Series E, 198; Kluwer: Dordrecht 1991.

(11) Musin, R. N.; Schastnev, P. V.; Malinovskay, S. A. In *Trends in Applied Theoretical Chemistry*; Montero, L. A., Smeyers, Y. G., Eds.; Kluwer Academic: Dordrecht, 1992; p 167.

(12) (a)Miralles, J.; Daudey, J. P.; Caballol, R. *Chem. Phys*. **1992**, *198*, 555. (b) Okumura, M.; Yamaguchi, K.; Awaga, K. *Chem. Phys. Lett*. **1994**, *228*, 575.

(13) Barone, V.; Bencini, A.; di Matteo, A. *J. Am. Chem. Soc*. **1997**, *119*, 10831.

(14) (a) Rega, N.; Cossi, M.; Barone, V. *J. Chem. Phys*. **1996**, *105*, 11060. (b) Rega, N.; Cossi, M.; Barone, V. *J. Am. Chem. Soc*. **1997**, *119*, 12962. (c) Rega, N.; Cossi, M.; Barone, V. *J. Am. Chem. Soc*. **1998**, *120*, 5723.

(15) (a) Amovilli, C.; Barone, V.; Cammi, R.; Cances, R.; Cossi, M.; Mennucci, B.; Pomelli, C. S.; Tomasi, J. *Adv. Quantum Chem*. **1998**, *32*, 227. (b) Cossi, M.; Barone, V.; Cammi, R.; Tomasi, J. *Chem. Phys. Lett*. **1996**, *255*, 327. (c) Cossi, M.; Barone, V. *J. Phys. Chem. A* **1998**, *102*, 1995. (d) Cossi, M.; Barone, V. *J. Chem. Phys.* **1998**, *109*, 6246.

(16) Burkert, U.; Allinger, N. L. *Molecular Mechanics*; American Chemical Society, Washington, DC, 1982.

(17) Cornell, W. D.; Cieplak, P.; Bayly, C. I.; Gould, I. R.; Merz, K. M., Jr.; Ferguson, D. M.; Sellmeyer, D. C.; Fox, T.; Caldwell, J. W.; Kollman, P. A. *J. Am. Chem. Soc*. **1995**, *117*, 5179.

(18) (a) Yamaguchi, K.; Okamura, M.; Maki, J.; Noro, T.; Namimoto, H.; Nakano, M.; Fueno, T.; Nakatsuji, K. *Chem. Phys. Lett*. **1992**, *190*, 353. (b) Okamura, M.; Yamaguchi, K.; Nakano, M.; Mori, W. *Chem. Phys. Lett*. **1993**, *207*, 1. (c) Castell, O.; Caballol, R.; Subra, R.; Grand, A. *J. Phys. Chem*. **1995**, *99*, 154. (d) Barone, V.; di Matteo, A.; Mele, F.; Moreira, I. de P. R.; Illas, F. *Chem. Phys. Lett*. **1999**, *302*, 240. (e) Barone, V.; Bencini, A.; Ciofini, I.; Daul, C. *J. Phys. Chem. A* **1999**, *103*, 4275.

(19) (a) Hart, J. R.; Rappé, A. K.; Gorun, S. M.; Upton, T. M. *J. Phys. Chem*. **1992**, *96*, 6255, 6264. (b) Ruiz, E.; Alemany, P.; Alvarez, S.; Cano, J. *Inorg. Chem*. **1997**, *36*, 3683. (c) Ruiz, E.; Alemany, P.; Alvarez, S.; Cano, J. *J. Am. Chem. Soc.* **1997**, *119*, 1297. (d) Ruiz, E.; Cano, J.; Alvarez, S.; Alemany, P. *J. Am. Chem. Soc*. **1998**, *120*, 11122. (e) Barone, V.; Bencini, A.; Ciofini, I.; Daul, C. A.; Totti, F. *J. Am. Chem. Soc*. **1998**, *120*, 8357. (f) Illas, F.; Martin, R. L. *J. Chem. Phys*. **1998**, *108*, 2519. (g) Adamo, C.; Barone, V.; Bencini, A.; Totti, F.; Ciofini, I. *Inorg. Chem*. **1999**, *38*, 1996.

(20) Bencini, A.; Totti, F.; Daul, C. A.; Doclo, K.; Fantucci, P.; Barone, V. *Inorg. Chem*. **1997**, *36*, 5022.

(21) (a) Noodleman, L.; Davidson, E. R. *Chem. Phys*. **1979**, *70*, 4903. (b) Noodleman, L. *J. Chem. Phys*. **1981**, *74*, 5737.

(22) Davidson, E. R.; Silver, D. W. *Chem. Phys. Lett*. **1997**, *52*, 403.

(23) Noodleman, L.; Norman, J. G. *J. Chem. Phys*. **1979**, *70*, 4903.

(24) Yamaguchi, K.; Jensen, F.; Dorigo, A.; Houk, K. N. *Chem. Phys. Lett*. **1988**, *149*, 537.

(25) Ovchinnikov, A. A.; Labanowski, J. K. *Phys. Rev. A* **1996**, *53*, 3946.

(26) Caballol, R.; Castell, O.; Illas, F.; Malrieu, J. P.; Moreira, I. de P. R. *J. Phys. Chem. A* **1997**, *101*, 7860.

(27) Pauncz, R. *Spin Eigenfucnctions: Construction and Use*; Plenum: New York, 1979.

(28) Barone, V. In *Recent Advances in Density Functional Methods*; Chong, D. P., Ed.; World Scientific: Singapore, 1995; p 287.

(29) Frisch, M. J.; Trucks, G. W.; Schlegel, H. B.; Scuseria, G. E.; Stratmann, R. E.; Burant, J. C.; Dapprich, S.; Millam, J. M.; Daniels, A. D.; Kudin, K. N.; Strain, M. C.; Farkas, O.; Tomasi, J.; Barone, V.; Cossi, M.; Cammi, R.; Mennucci, B.; Pomelli, C.; Adamo, C.; Clifford, S.; Ochterschi, J.; Cui, Q.; Gill, P. M. W.; Johnson, B. G.; Robb, M. A.; Cheeseman, J. R.; Keith, T.; Petersson; Morokuma, K.; Malick, D. K.; Rabuck, A. D.; Montgomery, J. A.; Raghavachari, K.; Al-Laham, M. A.; Zakrewski, V. G.; Ortiz, J. V.; Foresman, J. B.; Cioslowski, J.; Stefanov, B. B.; Nanayakkara, A.; Liu, J.; Liashenklo, A.; Piskorz, P.; Komaromi, I.; Challacombe, M.; Peng, C. Y.; Ayala, P. Y.; Chen, W.; Wong, M. W.; Andres, J. L.; Replogle, E. S.; Gomperts, R.; Martin, R. L.; Fox, D. J.; Binkley, J. S.; DeFrees, D. J.; Baker, J.; Stewart, J. P.; Head-Gordon, M.; Gonzalez, C.; Pople. J. A. *Gaussian 98*, revision A.6; Gaussian Inc.: Pittsburgh, PA, 1998.

(30) Hay, P. J.; Wadt, W. R. *J. Chem. Phys*. **1985**, *82*, 284.

(31) Description of basis sets and standard computational models can be found in the following. Foresman, J. B.; Frisch, *Æ. Exploring Chemistry with Electronic Structure Methods*, 2nd ed.; Gaussian Inc.: Pittsburgh, PA 1996.

(32) (a) Kohn, W.; Sham, L. *J. Phys. Rev. A* **1965**, *140*, 1133. (b) Slater, J. C. *Quantum Theory of Molecules and Solids. The Self-consistent Field for Molecules and Solids*; McGraw-Hill: New York, 1974; Vol. 4. (c) Vosko, S. H.; Wilk, L.; Nusair, M. *Can. J. Phys*. **1980**, *58*, 1200.

(33) Becke, A. D. *Phys. Rev. B* **1988**, *38*, 3098.

(34) Perdew, J. P. In *Proceedings of the 21st Annual International Symposium on the Electronic Structure of Solids*; Ziesche, P., Eschring, H., Eds.; Akademic Verlag: Berlin, 1991.

(35) Lee, C.; Yang, W.; Parr, R. G. *Phys. Rev. B* **1988**, *37*, 785.

(36) Perdew, J. P.; Wang, Y. *Phys. Rev*. **1992**, *B45*, 13244.

(37) Becke, A. D. *J. Chem. Phys*. **1993**, *98*, 5648.

(38) (a) Adamo, C.; Barone, V.; di Matteo, A. *Adv. Quantum Chem*., in press. (b) Adamo, C.; Barone, V. *Chem. Phys. Lett*. **1997**, *274*, 242. (c) Adamo, C.; Barone, V. *J. Chem. Phys*. **1998**, *108*, 627.

(39) Perdew, J. P.; Ernzerhof, M.; Burke, K. *J. Chem. Phys*. **1996**, *105*, 9982.

(40) Daudey, J. P.; Malrieu, J. P.; Maynau, D.; Pellissier, M.; Spiegalman, F.; Caballol, R.; Evangelisti, S.; Illas, F.; Rubio, J. PSH-CIPSI program package.

(41) Allinger, N. L. *J. Am. Chem. Soc.* **1977**, *99*, 8127 and subsequent versions, e.g., MM2-87, MM2-89, MM2-91.

(42) Barone, V.; Bencini, A.; Cossi, M.; di Matteo, A.; Mattesini, M.; Totti, F. *J. Am. Chem. Soc*. **1998**, *120*, 7069.

(43) HyperChem, release 3 for Windows, Hypercube Inc.

(44) Dickman, M. H.; Doedens, R. J. *Inorg. Chem*. **1981**, *20*, 2677.

(45) Rohmer, M. M.; Grand, A.; Benard, M. *J. Am. Chem. Soc*. **1990**, *112*, 2875.

(46) Huron, B.; Malrieu, J. P.; Rancurel, P. *J. Chem. Phys*. **1973**, *58*, 5745.

(47) Capiomont, A.; Lajzerowicz-Bonneteau, J. *Acta Crystallogr*. **1974**, *B30*, 2160.

(48) Lim, Y. Y.; Drago, R. S. *Inorg. Chem*. **1972**, *11*, 1334.

(49) Bayly, C.; Cieplak, P.; Cornell, W.; Kollman, P. A. *J. Phys. Chem*. **1993**, *97*, 10269.